Contact Mechanics and Fluid Leakage Near Percolation

W. B. Dapp, M. H. Müser

published in

NIC Symposium 2016
K. Binder, M. Müller, M. Kremer, A. Schnurpfeil (Editors)

Forschungszentrum Jülich GmbH,
John von Neumann Institute for Computing (NIC),
Schriften des Forschungszentrums Jülich, NIC Series, Vol. 48,
ISBN 978-3-95806-109-5, pp. 21.
http://hdl.handle.net/2128/9842

Contact Mechanics and Fluid Leakage Near Percolation

Wolf B. Dapp and Martin H. Müser

John von Neumann Institute for Computing and Jülich Supercomputing Centre,
Institute of Advanced Simulation, Forschungszentrum Jülich, 52425 Jülich, Germany
E-mail: {w.dapp, m.mueser}@fz-juelich.de

In this work, we present calculations on the leakage of fluid through the gap that forms between a rigid substrate with microscopic roughness and a flat but elastically deformable counter body that is pressed against the substrate. We find that the resistance to flow near the percolation threshold is determined by one, or at most very few constrictions. These constrictions can be described as saddle points and their contact mechanics determine the critical flow rather than the gap topography at large scales.

1 Introduction

The leak rate of simple fluids through an interface formed by a seal and a rigid, randomly rough surface decreases roughly exponentially with intermediate loads L squeezing seal and surface together[1–3]. At very high loads, the flow falls off even more quickly with L and eventually comes to a complete stop. The accepted picture is that beyond a threshold load, no more percolating open channel exists in which the fluid can pass from one side of the contact to the opposite side[4–6]. The analysis of the leak-rate problem has gained recent momentum mainly for two reasons: the contact mechanics theory by Persson[7] allows one to make quantitative predictions – also for the leakage of seals[2–4,8] – with little numerical effort. Large-scale computer simulations[5,6,9–11] have likewise progressed due to algorithmic developments and an increase in computing power making it possible to simulate ever more complex systems.

To describe theoretically the leak-rate of (static) seals, Persson and coworkers have pursued two approaches. One[2] is based on the idea that close to percolation all fluid pressure falls off at the constriction interrupting the last percolating channel at the critical load L_c. The topography of this critical constriction and thus its flow resistance is determined with Persson's contact mechanics theory. The second approach[3] is footed on Bruggeman's effective medium theory. It allows one to estimate the resistance to Reynolds flow from the distribution of interfacial separations[12]. The latter can be deduced to high accuracy from Persson's contact mechanics theory[4,13,14].

Although the leak-rate theory of seals has successfully reproduced both experiments[2,3] and simulations[6] in the pressure range where flow is suppressed exponentially with L, it is questionable whether it also describes flow close to the percolation point. Investigations on this issue are presented in this contribution. We note that our problem differs from the random (on/off) resistance networks[15], or simple generalisations thereof, like the Lorentz[16] or Swiss cheese model, which are often seen as generic models for percolation. In those models, conductivity is finite or zero in a given bond or domain. In our percolation problem, the local conductivity evolves smoothly to smaller values as the load increases and continuously approaches zero when the local gap between seal and substrate closes.

2 Methods

To find a realistic channel geometry, we need to simulate contacts in which roughness scales over at least $2-3$ decades of spatial scale. In order to make predictions that can be compared to continuum theory, the smallest lengthscale has to be sufficiently discretised, which adds another decade (away from the percolation threshold) or even more near the percolation point. Thus, in a brute-force analysis of the problem, the linear length of the system can be easily 10^5 discretisation points long, which boils down to 10^{10} surface grid points in a Fourier-based boundary element method like Green's function molecular dynamics (GFMD)[17]. Modern multi-scale methods that are not based on (fast) Fourier transforms cannot handle the problem more efficiently, due to the complexity of real contact (except at very small contact pressures, when contact is only formed at an isolated mesoscale asperity) and the long-range nature of elastic interactions. Last but not least, solving Reynolds' thin-film equation on a given domain can entail lengthy computations, whose solution time increases with the complexity of the open channel structure unless efficient solution strategies are pursued. In the following, we summarise the numerical methods we use.

General setup. We consider a system where there is a reservoir of liquid on one side, with a fluid pressure of 1, and on the other there is a sink for said liquid, with a pressure of 0. In the transverse direction the system is periodic. Since the choice of which direction is vertical and which one is horizontal is arbitrary, for each surface we also calculate the flow through the corresponding contact with a transposed surface. In addition, we also compute the flow through a contact where the surface is inverted. We performed these calculations for 6 different surfaces (with different random seeds).

Main aspects pertaining to contact mechanics. The liquid has to pass through channels created by pressing a rigid, randomly rough and a compliant, smooth surface against one another. The surfaces are created by treating the Fourier coefficients of the height spectra as (complex) random numbers whose first moment disappears and whose second moments satisfy

$$\langle \tilde{h}(\mathbf{q})\tilde{h}^*(\mathbf{q})\rangle \propto q^{-2(1+H)}\Theta(q_\mathrm{s}-q), \tag{1}$$

where H is the Hurst roughness exponent and $q_\mathrm{s}=2\pi/\lambda_\mathrm{s}$ with λ_s being the cutoff at short wavelengths. The elastic side is pressed against this substrate but not allowed to penetrate it via a hard-wall constraint. The displacement is considered as a scalar, with all lateral displacements neglected. Details can be found in the literature[18].

Main aspects related to computing the flow. We calculate the fluid flow using the stationary Reynolds thin-film equation. This means that each point in the interface is assigned a conductivity that scales as the third power of the interfacial separation. The `hypre` package[19] together with GMRES (generalised minimal residual) methods[20] and multigrid preconditioners is used to solve the sparse discretised Reynolds equation. Our in-house code is MPI-parallelised and uses HDF5 for I/O.

Scaling tests. Both GFMD and our Reynolds solver scale well with the number of processors. This is demonstrated in Fig. 1, where we show the extrapolated time it would take

one MPI rank to make one time step per particle or one iteration per grid point as a function of the requested nodes. In GFMD, this time is around $\gtrsim 1.3\,\mu$s with a cumulative loss of efficiency of a factor of $\lesssim 2$ when increasing the number of cores. The FFTW library decomposes the domain of a 2-dimensional Fourier transform into stripes. We find that below a stripe width of 16, the efficiency plummets because communication starts to dominate. This, together with the limit of 16 GiB of memory per JUQUEEN node limits the maximum system size we can tackle to $524,288$ grid cells in linear direction, using $65,536$ cores. A different FFT library with a different domain decomposition may remove this limitation, and allow the GFMD code to scale across the entire JUQUEEN. The number of iterations needed to reach convergence does not depend strongly on the system size, and the complexity of each step scales with $\mathcal{O}(N \log N)$. Each grid point requires ≈ 128 Byte of memory.

The Reynolds solver uses `hypre`, which is parallelised using a square domain decomposition. We find it ceases to scale well if each processor works on less than 512×512 grid points. At this workload per processor, compared to larger squares, the efficiency has dropped by only $\lesssim 20\%$. However, the number of steps to reach convergence increases with increasing system size and complexity, and thereby sets limits on the maximum problem size. The memory demands per grid point of the Reynolds solver are greater than that of GFMD by about a factor of 2 to 4, depending on the specific solver used.

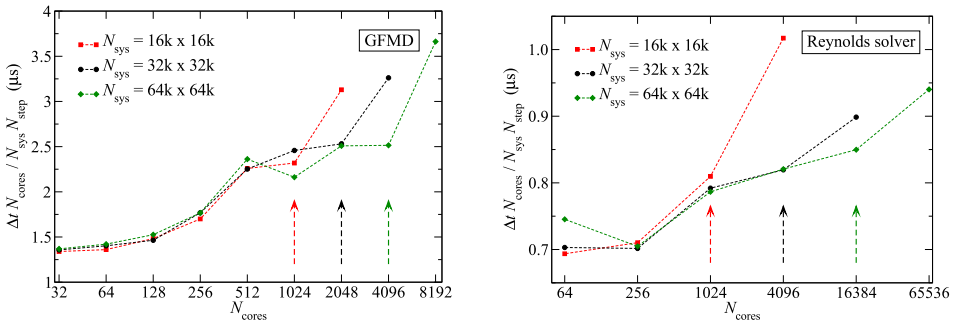

Figure 1. Strong scaling test of GFMD simulations (left) and the Reynolds solver (right) run on JUQUEEN for system sizes of $N_{\mathrm{sys}} = 16,384^2, 32,768^2$, and $65,536^2$. The abscissae correspond to the number of MPI ranks, N_{cores}, while the ordinates show the extrapolated time it would take one core to propagate one grid point by one time step. Here, Δt stands for the wall-clock time and N_{step} for the number of time steps or iterations. The arrows indicate a stripe width of 16 (for GFMD), and 512×512 grid points per process (Reynolds).

3 Results

3.1 Flow through Gaps Between Seals and Self-Affine Rough Surfaces

As the initial step of our simulations, we determine the critical load L_{c}, which is the external load L squeezing the seal against the self-affine rough surface, above which no more open fluid channel percolates through the system. We find (for a Hurst exponent of $H = 0.8$, which is a typical value for technical and natural surfaces alike) that L_{c} is the

load needed to induce a relative (critical) contact area of $a_{\mathrm{r}}^{*} = 0.413 \pm 0.018$. This result is in line with our previous estimate[6] of $a_{\mathrm{r}}^{*} = 0.42 \pm 0.02$. While this value may seem remarkably close to the value of ≈ 0.4073 for a square random site-percolation model, there is no *a priori* reason why the result should be the same, because the self-affine roughness induces long-range correlations in the surfaces that are not present in a random-site model. Additionally our contacts live on a continuum, which we represent by resolving the smallest wavelength in our system by many points. Their number increases from 4 far from the percolation threshold to 128 close to it.

Well below the critical load, i.e., at $1 - L/L_{\mathrm{c}} \gtrsim 0.2$, we find that the fluid current drops roughly exponentially with the load. For larger loads, i.e., in the vicinity of the percolation threshold, see also reference[21], the fluid current j disappears according to

$$j \propto (L_{\mathrm{c}} - L)^{\beta} \tag{2}$$

with $\beta \approx 7/2$. The exponent is deduced from data such as that shown in Fig. 2.

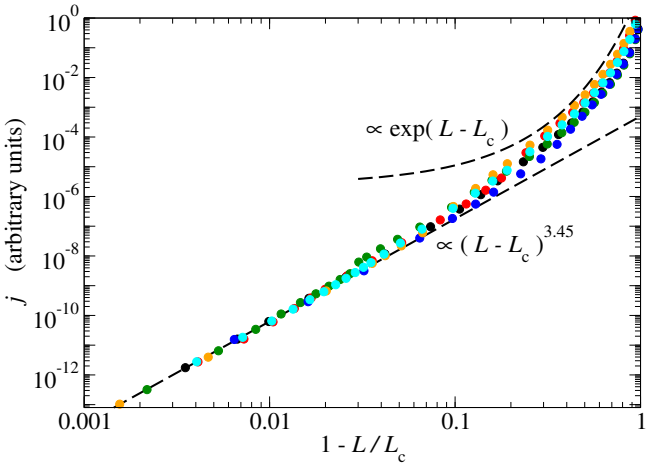

Figure 2. Disorder-averaged fluid flow j as a function of the reduced load $\Delta L = 1 - L/L_{\mathrm{c}}$. Differently coloured symbols represent different random realisations. For clarity not all available data sets are included in the figure, but they all show the same critical behaviour. The data are shifted vertically by a factor of up to $\lesssim 7$ to make them superimpose in the critical region.

To rationalise this behaviour, it is instructive to visualise the fluid flow. This is done in Fig. 3. It shows that the assumption of the critical junction theory appear to be valid, i.e., the fluid pressure drops in quasi-discrete jumps at narrow constrictions. In-between two constrictions, the fluid pressure is essentially constant.

3.2 Critical Flow in Isolated Constrictions

To rationalise the critical flow in the previous section, we now focus on isolated constrictions (see also Ref. 22). These are realised by single-wavelength substrate geometries. The

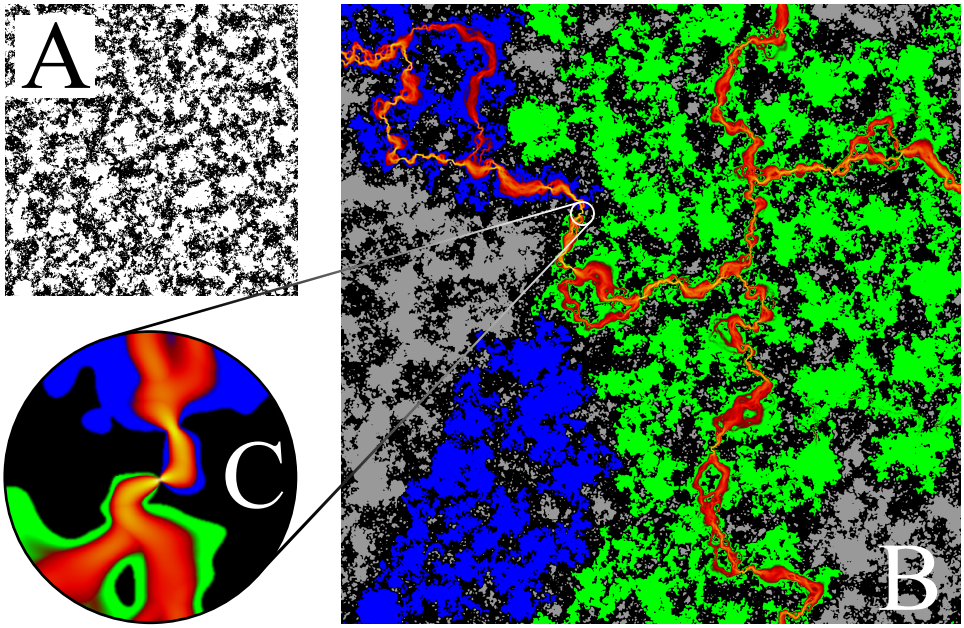

Figure 3. Visualisation of flow passing through the gap between a linearly elastic seal and a self-affine rough substrate (top-down view). **A:** true contact (black) near the percolation threshold. **B:** Flow pattern through the seal. Grey colour marks all non-contact regions that do not belong to the percolating fluid channel. Blue and green colours indicate the fluid pressure, which drops from one (blue) on the left border of the interface to zero (green) on the right border. Red and yellow hues indicate the absolute value of the fluid current density. **C:** Zoom onto the critical constriction.

simplest considered geometry is the square lattice, i.e., a height profile given by

$$\frac{h_{\mathrm{sq}}(x,y)}{h_0} = 2 + \cos\left(\frac{2\pi x}{\lambda}\right) + \cos\left(\frac{2\pi y}{\lambda}\right), \tag{3}$$

for which the simulation cell dimensions along x and y direction are chosen to coincide with the wavelength λ of the height undulation, that is $L_x = L_y = \lambda$. For the realisation of the hexagonal and its dual triangular lattice, we refer to the literature[22]. Here, we only note that their scaling is similar to that of square lattice, although critical contact areas differ quite substantially, as do the load ratios $r_{\mathrm{L}} \equiv L_{\mathrm{c}}/L_{\mathrm{f}}$, where L_{f} is the load needed to go into full contact, while L_{c} is the critical load at which the contact area percolates. We found the following numerical values for the relative contact area needed for percolation $a_{\mathrm{c}}(\mathrm{sq}) = 0.40185(6)$, $a_{\mathrm{c}}(\mathrm{tri}) = 0.17826(11)$, and $a_{\mathrm{c}}(\mathrm{hex}) = 0.67323(1)$. The load ratios were $r_{\mathrm{L}}(\mathrm{sq}) = 4$, $r_{\mathrm{L}}(\mathrm{hex}) = 30$, and $r_{\mathrm{L}}(\mathrm{tri}) = 1.4$.

In Fig. 4, we confirm the critical exponent that we found in the fractal case, and test how well Bruggeman theory describes the flow through an isolated constriction. A mean-field approach cannot reasonably be expected to describe critical behaviour, and indeed, as expected, it fails to predict flow accurately near the percolation threshold.

Since all three investigated saddlepoints have one positive and one negative height curvature, they show universal scaling of width, length, and height of the constriction with

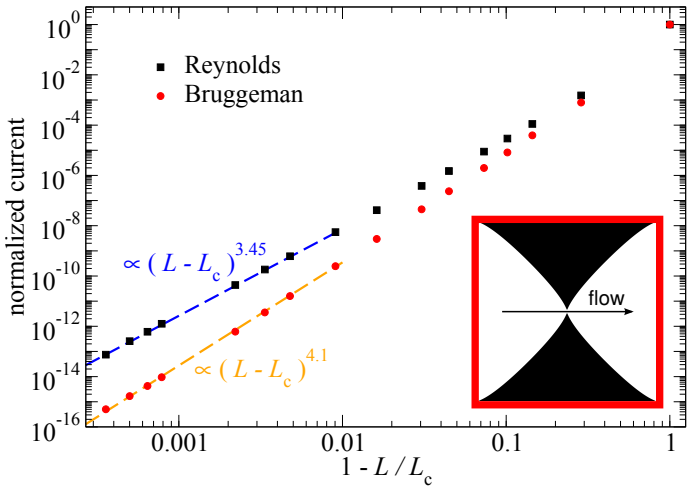

Figure 4. Reynolds flow through a square saddle-point constriction (described by Eq. 3). The inset illustrates the flow, where black is contact and white is a non-zero gap. The power law exponent is the same as for the fractal surface, while the Bruggeman mean field approximation predicts a slightly different scaling.

load

$$g(l, x, y) = |l|^{\zeta} g^{\pm}\left(\frac{x}{|l|^{\chi}}, \frac{y}{|l|^{\upsilon}}\right), \tag{4}$$

where $l = (L - L_c)/L_c$ is the reduced load and $g^{\pm}(\dots)$ are two master functions depending on whether the critical points is approached from high pressures or low pressures. The scaling exponents turn out $\zeta = 6/5$, $\chi = 3/5$, and $\upsilon = 9/20$, which means that they naturally lead to the observed exponent for the Reynolds flow of $\beta = 3\zeta + \upsilon - \chi = 69/20$. Only the prefactors and scaling factors depend on the ratio of positive and negative surface curvature.

Fig. 5 demonstrates this scaling relation. It shows the contact line in the x–y-plane (top-down view on the contact) in the left panel, and the shape of the gap in the right panel (x–z-plane, side-view of the contact), very close to the critical point ($l \leq 2\%$). The red and blue solid curves are the master functions $g^{\pm}(\dots)$ of Eq. 4, which both asymptotically approach the critical green curve. Different symbols show different saddle-point geometries, where we omit the hexagonal case, for clarity, and do not overplot the symbols on all legs of the curves. For all negative reduced loads l (i.e., $L < L_c$) and all geometries the points can be scaled to fall exactly on the blue curve, while for positive reduced loads ($L > L_c$), the red curve is the pertinent curve. Exactly *at* the critical point, the green curve is traced by the data.

This universality is the reason why the critical behaviour in the fractal case is the same for any of the random realisations we studied, even though the shape of the last constriction might be very different in every case. We note, however, that the precise *magnitude* of the leakage current *does* depend on the local geometry. Hence it remains impossible to predict the prefactor of the flow, just its scaling.

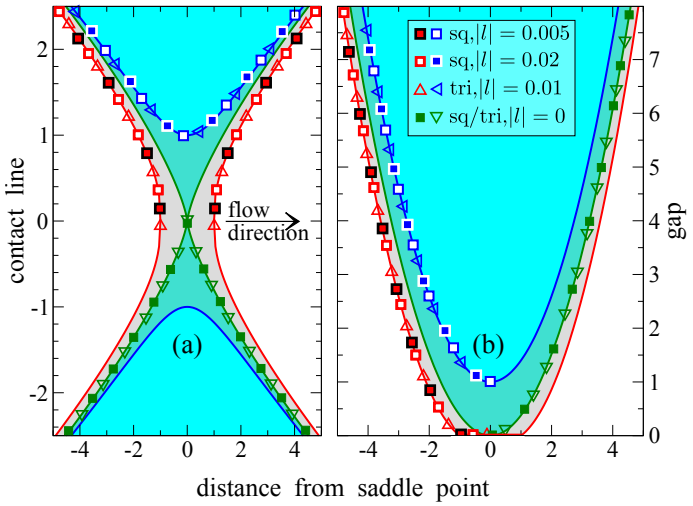

Figure 5. **(a)** Contact line shape for normal loads below (blue), at (green), and, above (red) the critical load. **(b)** Gap on the symmetry axis as a function of the distance from the saddle point. Different symbols represent different saddle-point geometries and different colours different reduced loads l, as indicated in the caption. Solid areas and lines are obtained from analytical approximations to the contact shape. At a given value of l, distances are rescaled according to Eq. 4. Units are chosen such that gap height, length, and width are 1 for $|l| = 0.01$ in the square model. From Ref. 22: Wolf B. Dapp & Martin H. Müser *Contact mechanics of and Reynolds flow through saddle points: On the coalescence of contact patches and the leakage rate through near-critical constrictions*, EPL 109 (2015) 44001. Reprinted with permission.

4 Conclusions

In summary, we carried out numerical simulations of contact between an elastic body with a rigid substrate with self-affine roughness, and computed the fluid flow through the resulting network of narrow channels. We find that, if one stays far enough away from the percolation point, Persson theory in combination with Bruggeman theory accurately predicts the leakage to be exponentially decreasing with external load. As the critical point is approached, at loads of $L \gtrsim 0.9\, L_\mathrm{c}$, essentially all fluid pressure drops at a single constriction. Then, the dependence of the current on load becomes a powerlaw, as the last constriction determines the resistance of the entire seal. Unsurprisingly, this is not well described by mean-field theory, and detailed calculations are necessary to compute the flow. We found the powerlaw exponent to be $\beta = 69/20$, and confirmed and rationalised this for single-wavelength saddle-point geometries. Independent on the curvature radius of the constriction, we obtain the same shape of the gap, which causes the universal scaling behaviour of the resistance.

However, the precise magnitude of the current does depend on the geometry, as that sets the prefactor of the powerlaw. As such, it is impossible to predict not only at what mechanical load or pressure a seal (like a faucet) stops dripping but also how it stops dripping unless detailed calculations are carried out for a specific (disorder realisation of the) surface. The situation can become even more complex as the universality class can change when additional features are included into the model such as adhesion between the surfaces or more realistic flow boundary conditions.

Acknowledgements

We gratefully acknowledge computing time on JUQUEEN at the Jülich Supercomputing Centre.

References

1. G. Armand, J. Lapujoulade, and J. Paigne, *A theoretical and experimental relationship between the leakage of gases through the interface of two metals in contact and their superficial micro-geometry*, Vacuum, **14**, 53–57, 1964.
2. B. Lorenz and B. N. J. Persson, *Leak rate of seals: Comparison of theory with experiment*, EPL, **86**, 44006, 2009.
3. B. Lorenz and B. N. J. Persson, *Leak rate of seals: Effective-medium theory and comparison with experiment*, Eur. Phys. J. E, **31**, 159, 2010.
4. B. N. J. Persson and C. Yang, *Theory of the leak-rate of seals*, J. Phys. Condens. Matter, **20**, 315011, 2008.
5. F. Bottiglione, G. Carbone, L. Mangialardi, and G. Mantriota, *Leakage mechanism in flat seals*, J. Appl. Phys., **106**, 104902, 2009.
6. W. B. Dapp, A. Lücke, B. N. J. Persson, and M. H. Müser, *Self-affine elastic contacts: percolation and leakage*, Phys. Rev. Lett., **108**, 244301, 2012.
7. B. N. J. Persson, *Theory of rubber friction and contact mechanics*, J. Chem. Phys., **115**, 3840–3861, 2001.
8. M. Scaraggi, G. Carbone, B. N. J. Persson, and D. Dini, *Lubrication in soft rough contacts: A novel homogenized approach. Part I - Theory*, Soft Matter, **7**, 10395–10406, 2011.
9. F. Sahlin, R. Larsson, P. Marklund, A. Almqvist, and P. M. Lugt, *A mixed lubrication model incorporating measured surface topography. Part 2: roughness treatment, model validation, and simulation*, P. I. Mech. Eng. J-J Eng., **224**, 353, 2009.
10. C. Vallet, D.Lasseux, P.Sainsot, and H. Zahouani, *Real versus synthesized fractalsurfaces: Contact mechanics and transport properties*, Tribol. Int., **42**, 250–259, 2009.
11. M. Scaraggi, G. Carbone, and D. Dini, *Lubrication in soft rough contacts: A novel homogenized approach. Part I - Theory*, Soft Matter, **7**, 10407–10416, 2011.
12. B. N. J. Persson, *Relation between interfacial separation and load: A general theory of contact mechanics*, Phys. Rev. Lett., **99**, 125502, 2007.
13. C. Campañá, B. N. J. Persson, and M. H. Müser, *Transverse and normal interfacial stiffness of solids with randomly rough surfaces*, J. Phys.: Condens. Matter, **23**, 085001, 2011.
14. A. Almqvist, C. Campañá, N. Prodanov, and B. N. J. Persson, *Interfacial separation between elastic solids with randomly rough surfaces: Comparison between theory and numerical techniques*, J. Mech. Phys. Solids, **59**, 2355–2369, 2011.
15. I. Webman, J. Jortner, and M. H. Cohen, *Critical exponents for percolation conductivity in resistor networks*, Phys. Rev. B, **16**, 2593–2596, 1977.
16. S. K. Schnyder, M. Spanner, F. Höfling, T. Franosch, and J. Horbach, *Rounding of the localization transition in model porous media*, Soft Matter, **11**, 701–711, 2015.
17. C. Campañá and M. H. Müser, *Practical Green's function approach to the simulation of elastic semi-infinite solids*, Phys. Rev. B, **74**, 075420, 2006.

18. N. Prodanov, W. B. Dapp, and M. H. Müser, *On the contact area and mean gap of rough, elastic contacts: Dimensional analysis, numerical corrections and reference data*, Tribol. Lett., **53**, 433–448, 2014.
19. R.D. Falgout, J.E. Jones, and U.M. Yang, *The Design and Implementation of hypre, a Library of Parallel High Performance Preconditioners*, in: Numerical Solution of Partial Differential Equations on Parallel Computers, 2006.
20. Y. Saad and M. H. Schultz, *GMRES: A generalized minimal residual algorithm for solving nonsymmetric linear systems*, SIAM J. Sci. Stat. Comput., **7**, 856–869, 1986.
21. W. B. Dapp and M. H. Müser, *Fluid leakage near the percolation threshold*, in press, 2015.
22. W. B. Dapp and M. H. Müser, *Contact mechanics of and Reynolds flow through saddle points*, EPL, **109**, 44001, 2015.